

---

# Fine-Grained Visual Prompting

---

Lingfeng Yang<sup>1</sup>, Yueze Wang<sup>2</sup>, Xiang Li<sup>3\*</sup>, Xinlong Wang<sup>2</sup>, Jian Yang<sup>1\*</sup>

<sup>1</sup>Nanjing University of Science and Technology

<sup>2</sup>Beijing Academy of Artificial Intelligence, <sup>3</sup>Nankai University

{yanglf@njust, csjyang}@njust.edu.cn, {yzwang, wangxinlong}@baai.ac.cn  
xiang.li.implus@nankai.edu.cn

## Abstract

Vision-Language Models (VLMs), such as CLIP, have demonstrated impressive zero-shot transfer capabilities in image-level visual perception. However, these models have shown limited performance in instance-level tasks that demand precise localization and recognition. Previous works have suggested that incorporating visual prompts, such as colorful boxes or circles, can improve the ability of models to recognize objects of interest. Nonetheless, compared to language prompting, visual prompting designs are rarely explored. Existing approaches, which employ coarse visual cues such as colorful boxes or circles, often result in sub-optimal performance due to the inclusion of irrelevant and noisy pixels. In this paper, we carefully study the visual prompting designs by exploring more fine-grained markings, such as segmentation masks and their variations. In addition, we introduce a new zero-shot framework that leverages pixel-level annotations acquired from a generalist segmentation model for fine-grained visual prompting. Consequently, our investigation reveals that a straightforward application of blur outside the target mask, referred to as the Blur Reverse Mask, exhibits exceptional effectiveness. This proposed prompting strategy leverages the precise mask annotations to reduce focus on weakly related regions while retaining spatial coherence between the target and the surrounding background. Our **Fine-Grained Visual Prompting (FGVP)** demonstrates superior performance in zero-shot comprehension of referring expressions on the RefCOCO, RefCOCO+, and RefCOCOg benchmarks. It outperforms prior methods by an average margin of 3.0% to 4.6%, with a maximum improvement of 12.5% on the RefCOCO+ testA subset. The part detection experiments conducted on the PACO dataset further validate the preponderance of FGVP over existing visual prompting techniques. Code is available at <https://github.com/ylingfeng/FGVP>.

## 1 Introduction

The usage of Vision-Language models (VLMs) [42, 31, 1, 30] has become increasingly prominent in various vision-related tasks, largely due to their notable impact. These models benefit from a vast amount of training data and parameters, demonstrating powerful performance in the training of fundamental visual model backbones [34, 15, 51]. Moreover, the transfer learning potential of VLMs has been employed in tasks such as open vocabulary detection [20, 64], visual grounding [32, 37], and image editing [6, 5], etc.

In the above-mentioned works, the VLMs generally require additional training, to adapt to each specific downstream task. However, the utilization of off-the-shelf Vision-Language Models (VLMs)

---

\*Corresponding authors. Work is done during Lingfeng Yang’s internship at BAAI.

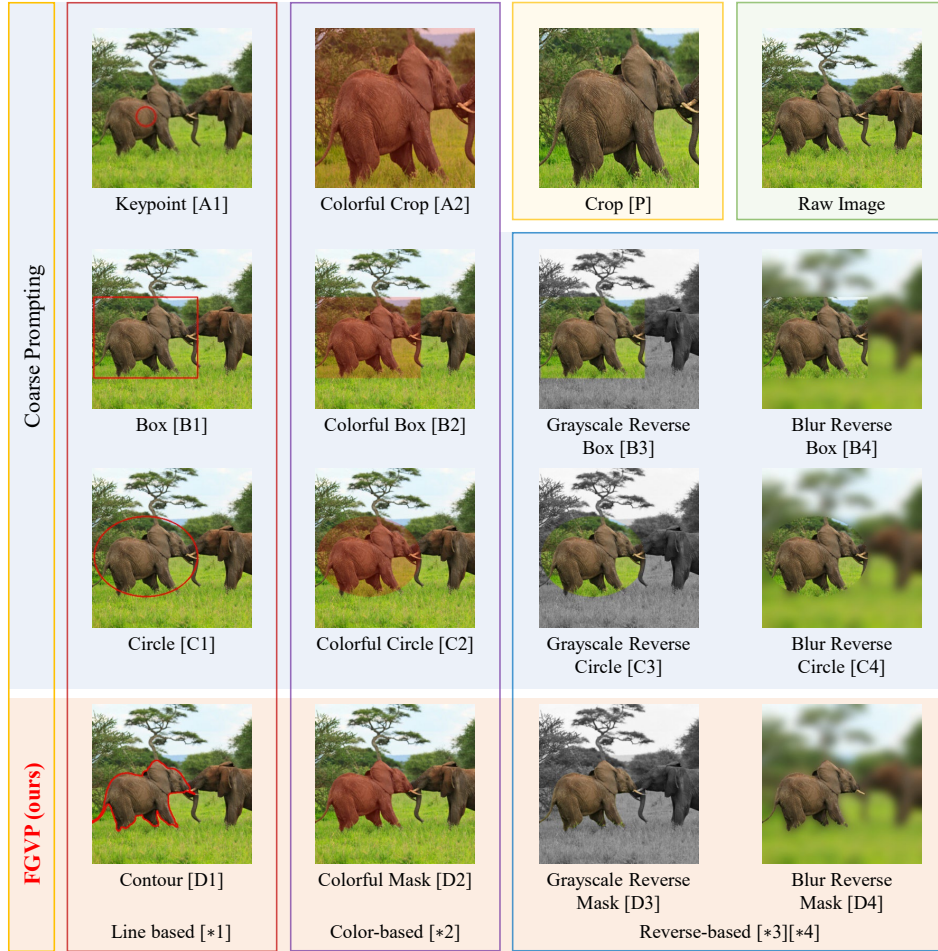


Figure 1: A Summary of visual prompts with the caption “elephant on the left”.

for leveraging their inherent image-text understanding, without additional tuning, remains largely unexplored. A notable challenge lies in the low sensitivity of VLMs to perform object spatial localization due to the presence of a large amount of weakly related background noise in the images [68, 3, 35]. The common practice involves cropping the region of interest [10, 62] to obtain a zoomed-in visual representation of a single object, at the expense of discarding valuable global information. As a result, existing training-free approaches for classification lack a comprehensive understanding of contextual information and spatial awareness across different objects.

In recent studies, CPT [61] and ReCLIP [50] have leveraged visual prompting techniques to establish relations between partial instances. Visual prompting is a technique used in image-language tasks, where markers such as colorful boxes or circles are added directly onto an image to highlight specific targets. By utilizing appropriate visual prompts, the attention of VLMs can be effectively directed toward the desired targets while preserving the global context. Moreover, a study by RedCircle [49] demonstrated that drawing red circles enclosing the object on the entire image can effectively distinguish instances, where the circles correspond to inscribed ellipses derived from proposal boxes. This discovery suggests that Vision-Language Models (VLMs) may possess the inherent ability to understand the local object within an overall image. Therefore, a specifically designed visual prompt has the potential to explicitly invoke this capability of VLMs, thereby benefiting various tasks.

Despite the interest in visual prompting techniques, their unique designs have yet to be fully explored. The current approaches only rely on coarse markers like colorful boxes or circles, which can introduce ambiguity and fail to highlight the intended instance accurately. In this paper, we address this issue by systematically organizing and investigating various forms of visual prompting. Further, we propose a refined technique called Fine-Grained Visual Prompting (FGVP), which utilizes semantic masks to mark each target precisely, thereby enhancing zero-shot performance.

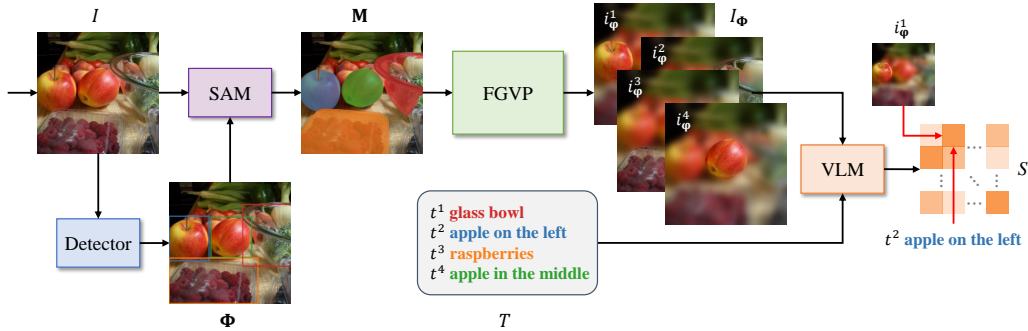


Figure 2: Structure of fine-grained visual prompting with box proposals from a detector.

In our research, we examine different visual prompting designs showcased in Fig. 1, including those utilized in previous studies such as CPT [61], ReCLIP [50], and RedCircle [40]. To provide an overview of previous research, we summarize their strategies in Table 1. It is important to note that some approaches achieve their best results through prompt ensembles or post processing techniques, which are discussed extensively in Sec. 3.1. Despite the progress made in visual prompting, none of the existing methods have fully explored the use of more precise semantic masks as fine-grained markers, rather than relying on coarse boxes or circles. To verify the effectiveness, we begin by exploring the upper bound of these prompts. Our methodology assumes perfect accuracy of all annotations applied, ensuring that images are marked with ground-truth information, namely bounding boxes and masks. We confirm that a *single* Blur Reverse Mask [D4], which involves blurring all content outside the instance mask, significantly outperforms other types of visual prompts on multiple datasets. This indicates the effectiveness of our fine-grained visual prompt design.

In practical scenarios where ground-truth annotations are unavailable, there are two primary approaches for obtaining fine-grained visual markings. The first approach is based on utilizing object proposals predicted by a pretrained detector, following a similar paradigm as employed in MAttNet [62]. This approach is commonly employed in zero-shot classification tasks [61, 50, 49]. To generate fine-grained masks, we employ Segment Anything Model (SAM) [26], which takes the aforementioned bounding boxes (refer to Fig. 2) as input prompts. Additionally, we propose a second approach that eliminates the dependency on a detector for prompt candidates. Our approach establishes a viable zero-shot pipeline by solely leveraging SAM, irrespective of specific tasks. Specifically, we prompt SAM with grid-wise keypoints and subsequently apply a non-maximum suppression (NMS) operation to obtain proposals with semantic masks. These fine-grained masks can then be employed for zero-shot classification (see Fig. 3).

Existing Method	Visual Prompt	Post Processing
MAttNet [62], UNITER [10]	$P$	–
CPT [61]	$A2$	–
ReCLIP [50]	$P \mid B4$	Relations [50]
RedCircle [40]	$C1 \mid C3 \mid C4$	Subtraction [40]

Table 1: The type of Visual Prompt equipped in previous works related to the referring expression comprehension task. “ $\mid$ ” denotes ensemble results of multiple prompts.

Our contributions can be summarized as follows:

- We propose Fine-Grained Visual Prompting (FGVP), employing Blur Reverse Masks to enhance the semantic localization capability of Vision-Language models such as CLIP (Fig. 1). To the best of our knowledge, we are the first to explore the use of Blur Reverse Masks as visual prompting, highlighting their remarkable effectiveness in zero-shot image-text comprehension.
- We are the first to provide a comprehensive exploration of visual prompt formats, including crop, box, circle, mask with different line markings, colored masks, grayscale, and Gaussian blurring. Additionally, we thoroughly analyze and evaluate the impact of associated auxiliary attributes such as blur deviation, color, etc., ensuring a comprehensive understanding of their effects.
- Our proposed Fine-Grained Visual Prompting (FGVP) achieves state-of-the-art (SOTA) zero-shot results on the referring expression comprehension task, surpassing ReCLIP and RedCircle by an average of 4.6% and 3.0% accuracy, respectively, across RefCOCO, RefCOCO+, and RefCOCOg benchmarks. Notably, our zero-shot pipeline demonstrates superior part detection accuracy on the PACO dataset compared to previous visual prompting methods.

## 2 Related Work

**Vision-Language Models** Large Language Models (LLMs), such as GPT-3 [7], GPT-4 [41], LLaMA [53], and PaLM [12], have demonstrated strong zero-shot transfer abilities in natural language processing. In recent years, vision-language Models (VLMs) that leverage image-text data pairs from the web have gained prominence in computer vision (CV) tasks. CLIP [42] and ALIGN [31] learn image-text alignment through contrastive learning. Furthermore, models like Flamingo [1] have shown impressive few-shot learning capabilities. BLIP-2 [30, 29] proposes joint multimodal task handling through transfer learning. Notably, VLMs have excelled in image-text generation as demonstrated by DALL-E [46, 45]. However, instance-level tasks such as referring expression comprehension and part detection typically require tuning of vision and text encoders in existing open vocabulary methods [20, 64] and image grounding approaches [32, 37]. In contrast, this paper proposes a zero-shot architecture for instance-level tasks using off-the-shelf VLMs.

**Prompt Engineering** Prompt engineering is a well-developed practice in NLP [43, 7]. Auto-Prompt [48] and CoOp [69] automate the generation of prompt templates, leveraging gradient-based methods instead of manual crafting. Language prompting is then extended to open vocabulary detection [14, 16] and segmentation [59]. While language prompting has been extensively explored, visual prompting has received less attention. Previous works [35, 22, 2, 4] use visual prompt tuning to adapt to VLMs. In terms of zero-shot solutions, CPT [61] introduces colorful boxes as markers on images, and RedCircle [49] demonstrates the effectiveness of a circle mark for visual attention during zero-shot classification. However, existing visual prompting methods lack fine-grained precision. In contrast, we propose leveraging semantic masks derived from segment models like Segment Anything [26] for more precise visual marking. It is worth noting that CPT [61] also employs semantic masks as colored prompts, but only after cropping the region using bounding boxes. In our approach, we directly mark the fine-grained mask on the entire image to preserve the global visual content.

**Image Segmentation** Image segmentation is a common task in computer vision [52], involving predicting region segment masks by labeling pixels. This task encompasses various sub-tasks such as instance segmentation [21, 13, 55], semantic segmentation [38, 67, 11], and panoptic segmentation [25, 25]. Recent advancements include SegGPT [56], which facilitates performing diverse segmentation tasks through in-context visual learning. Another notable approach, Segment Anything Model (SAM) [26], introduces spatial prompts for segmenting arbitrary objects. SAM is trained using an extensive dataset of over 1 billion segmentation masks. In our study, we employ the off-the-shelf SAM framework to generate precise semantic masks for fine-grained visual prompting.

**Referring Expression Comprehension** This task involves providing captions for specific objects in images and localizing them with bounding boxes. Proposal-based methods use object detectors like Mask R-CNN [21] to detect instance regions. Each proposal is then cropped and used for subsequent categorization. Examples include MAttNet [62], UNITER [10], OSCAR [33], and VinVL [66]. Proposal-free methods, such as MDETR [23] and ViLT [24], train Vision-Language Models end-to-end. Recent zero-shot methods [61, 50, 40] combine proposal boxes from MAttNet [62] with Vision-Language Models for image-caption matching. Our work follows this setup for fair comparisons.

**Part Detection** Part Detection is a sub-field of object detection [21, 47, 17, 8], primarily focused on fine-grained classification [65, 54] and human parsing [58, 18] that require precise region localization. Notable datasets include CUB-200 [54] for annotated bird parts, LIP [19] for semantic human part labels, PASCAL-Part [9] for common objects, and PACO [44], which introduces a comprehensive benchmark with jointly annotated part masks. Previous zero-shot works typically detect objects and parts using pre-annotated visual attributes to transfer the knowledge [28]. In contrast, we leverage the transferability of Vision-Language Models to perform part detection in this study.

## 3 Method

In this section, we begin by presenting a comprehensive overview of the visual prompting pipeline for zero-shot object recognition and part detection tasks. Subsequently, we delve into the details of our Fine-Grained Visual Prompting (FGVP) architecture. Finally, we examine the effectiveness and rationale behind our design.

### 3.1 Framework

The zero-shot framework takes as input an image  $I \in \mathbb{R}^{3 \times H \times W}$ ,  $N$  box proposals  $\Phi \in \mathbb{R}^{N \times 4}$  and  $M$  caption texts  $T \in \Omega^M = \{t^1, t^2, \dots, t^M\}$ , where  $\Omega$  denotes the set of textual sentences. The goal is to find the best matching image-text pairs. A common practice is to get each image input by cropping or RoIAlign [21] according to  $\Phi$ . However, with the introduction of visual prompting, one can mark the regions on the whole image, which highlights each target instance while keeping the background knowledge. For simplicity, we regard cropping as an ordinary type of visual prompting. Then the image input  $I_\Phi \in \mathbb{R}^{N \times 3 \times H \times W} = \{i_\Phi^1, i_\Phi^2, \dots, i_\Phi^N\}$  for VLMs can be generated as:

$$I_\Phi = \text{VP}(I, \Phi), \quad (1)$$

where  $\text{VP}$  concludes visual prompting, such as cropping, drawing colorful boxes or circles, or employing fine-grained masks, etc. Then the cosine similarity  $S = \{s(i_\Phi^n, t^m)\}_{N \times M}$  between each image proposal  $I_\Phi$  and text  $T$  can be derived by the VLM, e.g., CLIP [42]. For the referring expression comprehension task,  $T$  is a gathering of short sentences that describe the related instances in the image, and one needs to predict their referring location. Note that there exist some post processing techniques for this task, namely ‘‘Relations’’ [50] and ‘‘Subtraction’’ [49], respectively. The ‘‘Relations’’ considers spatial relations  $R = \{r(i_\Phi^{n_1}, i_\Phi^{n_2})\}_{N \times N}$  between every two proposals, w.r.t. left, right, above, below, bigger, smaller, and inside. Then the parsed final scores are updated as:

$$S = \{\sum_{i_\Phi^{n'} \in I_\Phi} (s(i_\Phi^n, t^m) \cdot r(i_\Phi^n, i_\Phi^{n'})), s \in S, r \in R\}. \quad (2)$$

Besides, the ‘‘Subtraction’’ deals with positive and negative text set to weigh down the score. By randomly sampling  $Q$  negative captions  $\tilde{T}$  that related to no instances on the image, all negative scores are calculated as  $\tilde{S} \in \mathbb{R}^{N \times Q} = \{\tilde{s}(i_\Phi^n, \tilde{t}^q)\}$ . And then use it to penalize  $S$ :

$$S = \{s(i_\Phi^n, t^m) - \frac{1}{Q} \cdot \sum_{\tilde{t}^q \in \tilde{T}} \tilde{s}(i_\Phi^n, \tilde{t}^q), s \in S, \tilde{s} \in \tilde{S}\}. \quad (3)$$

Once the final scores are obtained, the referring region  $\hat{\Phi}$  can be given by:

$$\hat{\Phi} = \{\hat{\varphi} \mid \hat{\varphi} = \text{ARGMAX}_{i_\Phi^n \in I_\Phi} s(i_\Phi^n, t^m), s \in S\}. \quad (4)$$

For the part detection task, the text is the object or part label names. Considering the general case, each part only appears in one region (all eyes of a bird are covered by a single box). Thus we indicate a post processing strategy for this task with the Hungarian algorithm [27], to find a bipartite matching between image proposals and part labels. Otherwise, the label predicted corresponding to each proposal is derived as:

$$\hat{T} = \{\hat{t} \mid \hat{t} = \text{ARGMAX}_{t^m \in T} s(i_\Phi^n, t^m), s \in S\}. \quad (5)$$

### 3.2 Fine-Grained Visual Prompting

Existing visual prompts primarily use proposal boxes from the detector. The Crop [P] and Colorful Crop [A2] prompts involve extracting cutouts of the original image based on the location of the box. Prompting with Keypoint [A1] entails placing a small circle around the box center. The box-based [B\*] prompts naturally use the box as the marking boundary, while the circle-based [C\*] prompts are essentially similar to [B\*], except for replacing the box with its inscribed ellipse.

However, these prompts are too coarse to emphasize key targets. Marking inaccuracies introduce irrelevant information and lead to sub-optimal performance based on empirical evidence. We illustrate previous visual prompting approaches as coarse prompting on top of Fig. 1. In contrast, we investigate fine-grained visual prompting using semantic masks, which can accurately highlight the target instance, reduce background interference, and retain global knowledge. Nonetheless, obtaining semantic masks may pose a challenge when only proposal boxes are provided. To tackle this issue, we propose the use of a robust image segmentation model called Segment Anything Model (SAM) [26] to perform class-agnostic segmentation based on the given boxes (Fig. 2):

$$\mathbf{M} = \text{SAM}(I, \Phi), \quad (6)$$

$$I_\Phi = \text{FGVP}(I, \mathbf{M}), \quad (7)$$

where  $\text{SAM}$  denotes Segment Anything Model [26], and  $\mathbf{M} \in \mathbb{R}^{N \times H \times W}$  denotes the semantic masks. We updated Eq. (1) with Eq. (6), (7) to produce fine-grained visual prompting.

In addition, We innovatively proposed a zero-shot classification pipeline, which does not require pre-processed box proposals but directly generates fine-grained markers. The key idea lies in that

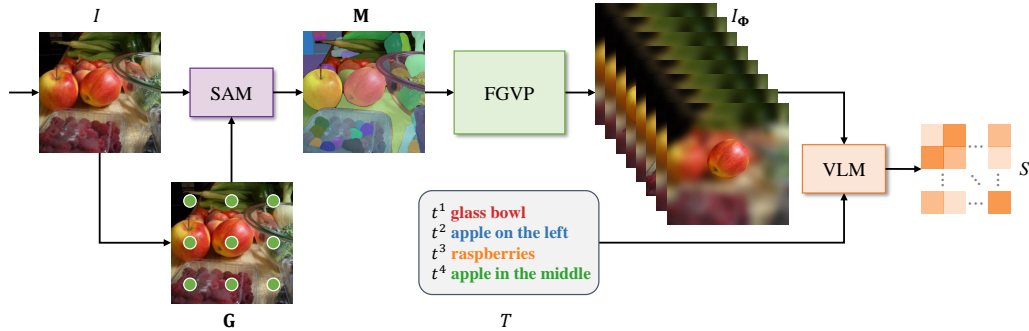


Figure 3: Structure of fine-grained visual prompting with no box proposal. Masks are directly derived via SAM prompted by grid-wise keypoints.

SAM can propose an extremely exhaustive prediction of almost any object or parts on the images taken a grid-wise set of keypoints  $\mathbf{G} \in \mathbb{R}^{g^2 \times 2}$  as inputs (Fig. 3), where  $g$  is the point number along one side of the image. Then the mask is generated through SAM prompted by the grid-wise keypoints:

$$\mathbf{M} = \text{NMS}(\text{SAM}(I, \mathbf{G})), \quad (8)$$

where NMS denotes Non-Maximum Suppression to filter out duplicate proposals. Notably, the regression box  $\Phi$  is obtained by calculating the smallest box containing the object mask.

Following the FGVP illustration, we provide an overview of all visual prompting variants. In addition to the categorization based on box, circle, and mask, they can also be sorted based on different markers, such as line [\*1], color [\*2], grayscale [\*3], and blur [\*4]. Specifically, line-based methods utilize closure lines to prompt the image, while color-based prompting involves drawing colorful masks on the target. These two types can be classified as positive marking, which aims to highlight the target area. Conversely, the reverse-based prompting serves as a form of negative marking by grayscaling or blurring the background area, thereby reducing the impact of weakly related information.

### 3.3 Discussion

In fact, both part detection and referring tasks require a mutual understanding between instances and backgrounds. In the referring expression comprehension task, captions are used to describe the interrelationships between multiple objects. Similarly, in part detection, a local part can be hard to classify regardless of the object. Successful performance of these tasks thus necessitates a network’s ability to handle global information and accurately comprehend the relationships between instances. For this reason, implementing more precise visual prompting is helpful, typically with the Blur Reverse Mask Prompting [D4]. This is because the web-scale dataset on which VLM is trained contains a large amount of photography.

These images prefer to employ “Bokeh” to blur the background and highlight the subject (Fig. 4). As a result, VLMs may have prior knowledge of visual prompting with background blurring.

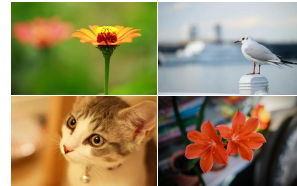


Figure 4: Photography from the Internet with “Bokeh”.

## 4 Experiments

In this section, we first evaluate individual visual prompting performance. Then, we compare FGVP with previous zero-shot methods on the referring expression comprehension and part detection tasks to show our effectiveness. For more experimental analysis refer to the Supplementary Materials.

### 4.1 Dataset

We conduct the experiments on several visual datasets, i.e., RefCOCO [63], RefCOCO+ [63], RefCOCOg [39], COCO [36], and PACO [44]. The RefCOCO, RefCOCO+, and RefCOCOg datasets are subsets selected from COCO, containing bounding boxes and masks corresponding to captioned

Visual Prompt	Ground Truth					Referring Expression Comprehension		
	COCO	PACO	RefCOCO	RefCOCO+	RefCOCog	RefCOCO	RefCOCO+	RefCOCog
Crop	<b>70.9</b>	38.5	35.2	40.3	59.1	45.3	46.4	56.4
Keypoint	52.3	39.1	36.9	39.6	43.8	46.7	47.9	48.9
Colorful Crop	64.2	35.7	37.1	41.9	58.0	48.2	49.0	<u>57.0</u>
Box	48.5	42.7	34.7	39.5	44.6	45.5	46.4	47.0
Colorful Box	34.4	37.2	23.9	23.4	22.7	35.4	30.7	30.8
Grayscale Reverse Box	42.4	37.4	34.4	35.9	44.5	45.9	44.0	48.4
Blur Reverse Box	62.1	39.2	47.9	51.8	<b>63.6</b>	48.8	51.4	54.1
Circle	48.9	42.6	43.2	49.3	56.3	48.9	51.7	54.6
Colorful Circle	36.1	37.2	29.9	29.8	24.5	40.7	37.1	37.9
Grayscale Reverse Circle	42.9	36.6	36.9	38.2	47.3	47.8	46.2	50.3
Blur Reverse Circle	58.1	36.8	<u>49.2</u>	<u>53.1</u>	60.9	<u>49.3</u>	<u>52.1</u>	52.2
Contour	47.3	41.0	38.7	41.7	43.5	46.1	45.0	46.3
Mask	41.1	<b>43.7</b>	29.9	29.1	29.9	41.8	38.5	38.4
Grayscale Reverse Mask	45.2	40.4	40.5	43.8	50.9	45.8	45.9	51.2
Blur Reverse Mask	<u>67.8</u>	<u>43.3</u>	<b>52.8</b>	<b>58.0</b>	<u>63.5</u>	<b>52.8</b>	<b>55.4</b>	<b>57.8</b>

Table 2: Ablation study on the zero-shot performance of individual visual prompting in the validation set of COCO, PACO, RefCOCO, RefCOCO+, and RefCOCog datasets using ground truth annotations (left) and proposals in referring expression comprehension (right), respectively. Best metrics are in **bold**, and sub-optimal results are underlined.

instances. The COCO dataset is annotated with boxes and masks for objects, while PACO additionally incorporates annotations of corresponding parts for each object.

## 4.2 Implementation Details

We follow Timm [57], CPT [61], and ReCLIP [50] to construct our pipelines. By default, we use ViT-B/32, ViT-L/14@336px, and RN50x16 backbones trained in CLIP [42] by OpenAI as our vision-language model. To simplify reference to these models in subsequent experiments, we refer to them as ViT-B, ViT-L, and RN. Additionally, for improved mask generalization, we employ SAM-ViT-H, a variant of Segment Anything Model [26]. Concerning part detection on the PACO [44] dataset, we begin by cropping the object according to the annotated boxes and then perform part detection on each object crop. All experiments are conducted on 8× Tesla V100.

## 4.3 Ablation Study on Visual Prompt

In this section, we elaborate on the zero-shot performance of individual visual prompts defined in Fig. 1 with two experiment settings. Firstly, we assume all prompting representations, i.e., bounding boxes and semantic masks, to be as precise as possible, in order to explore the upper bound of each visual prompt. Therefore, we acquire them from ground truth annotations of all datasets. Then we evaluate the image-label matching accuracy following the zero-shot pipeline described in Sec. 3.1. More specifically, instance-label pairs are represented as object-object name, part-part name, and object-caption in COCO, PACO, and RefCOCO series datasets, respectively. The left part of Table 2 reveals that the Blur Reverse Mask [D4] offers the best overall performance.

In the second part, we ablate on the referring expression comprehension task under the codebase of ReCLIP [50] with proposal boxes provided by MAttNet [62]. Note that in this setting, semantic

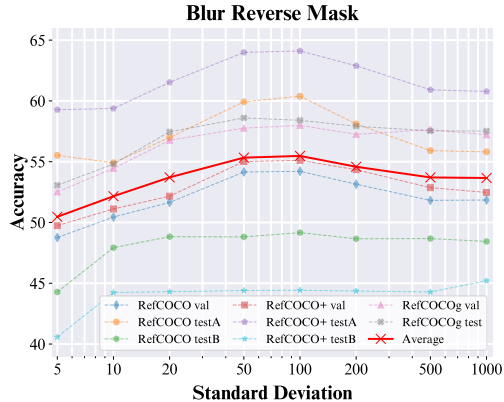


Figure 5: Ablation on the standard deviation in Gaussian blur kernel from the Blur Reverse Mask [D4] prompting. A larger deviation presents a more blurred background.

Method	Backbone	Visual Prompt	PP	RefCOCO			RefCOCO+			RefCOCOg	
				val	testA	testB	val	testA	testB	val	test
<i>Our codebase with object proposals detected by UNINEXT [60]</i>											
Crop	ViT-L	$P$	–	45.3	47.2	43.7	46.4	48.7	42.9	56.4	56.3
RedCircle [49] †	ViT-L	$C1$	–	48.9	56.4	41.3	51.7	59.5	41.8	54.6	54.7
FGVP (ours)	ViT-L	$D4$	–	<b>52.8</b>	<b>56.6</b>	<b>46.4</b>	<b>55.4</b>	<b>62.0</b>	<b>46.6</b>	<b>57.8</b>	<b>58.3</b>
<i>CPT [61] codebase with object proposals detected by MAttNet [62]</i>											
CPT [61]	VinVL [66]	$A2$	–	32.2	36.1	30.3	31.9	35.2	28.8	36.7	36.5
RedCircle [49] †	ViT-L	$C1$	–	38.0	45.3	32.9	43.9	51.0	37.1	47.2	47.3
FGVP (ours)	ViT-L	$D4$	–	<b>46.1</b>	<b>53.0</b>	<b>40.4</b>	<b>50.4</b>	<b>57.5</b>	<b>42.6</b>	<b>54.5</b>	<b>54.1</b>
<i>ReCLIP [50] codebase with object proposals detected by MAttNet [62]</i>											
CPT-adapted [50] ‡	ViT-B, RN	$B2$	R	23.2	21.4	27.0	23.9	21.6	25.9	22.3	23.7
CPT-adapted [50] ‡ †	ViT-B, RN	$P   B2$	R	41.3	40.6	44.0	41.3	41.8	41.1	51.3	51.2
ReCLIP [50]	ViT-B, RN	$P   B4$	R	45.8	46.1	47.1	47.9	50.1	45.1	59.3	59.0
RedCircle [49] †	ViT-B, RN	$P   C1$	R	43.9	46.2	44.1	45.3	47.9	43.1	57.3	56.3
FGVP (ours)	ViT-B, RN	$P   D4$	R	52.0	55.9	48.8	53.3	60.4	46.7	62.1	61.9
RedCircle [49]	ViT-L, RN	$C1   C3   C4$	S	49.8	58.6	39.9	55.3	63.9	45.4	59.4	58.9
RedCircle [49] †	ViT-L, RN	$C1   C3   C4$	S	51.4	58.3	40.9	56.3	63.6	45.8	58.3	58.0
FGVP (ours)	ViT-L, RN	$D1   D3   D4$	S	52.9	59.6	43.9	57.4	64.8	46.3	58.1	58.3
RedCircle [49] †	ViT-L, RN	$P   C1   C3   C4$	S	51.6	58.0	42.0	58.1	64.5	47.5	60.0	59.3
FGVP (ours)	ViT-L, RN	$P   D1   D3   D4$	S	53.9	60.2	44.3	59.3	66.6	48.8	61.0	61.3
RedCircle [49] †	ViT-L, RN	$P   C1   C3   C4$	RS	56.8	62.4	49.1	58.6	64.7	48.3	62.2	61.0
FGVP (ours)	ViT-L, RN	$P   D1   D3   D4$	RS	<b>59.6</b>	<b>65.0</b>	<b>52.0</b>	<b>60.0</b>	<b>66.8</b>	<b>49.7</b>	<b>63.3</b>	<b>63.4</b>

Table 3: The performance of the *rec* benchmarked with RefCOCO, RefCOCO+, and RefCOCOg datasets. The Visual Prompting strategies are shown in Fig. 1. **PP**: Post Processing, “R” and “S” denote Spatial Relations [50] and Score Subtraction [49], respectively. **FGVP**: Fine-Grained Visual Prompting. ‡CPT-adapted is an adapted version of CPT-Blk implemented by ReCLIP. † Re-implementation performance. The best result for each dataset, w.r.t. each codebase is in **bold**.

masks in FGVP are derived following our proposed framework presented in Fig. 2. Consequently, the Blur Reverse Mask [ $D4$ ] shows a consistent superiority demonstrated in the right part of Table 2. Notably, in line-based [ $*1$ ] prompting, we employ a default red line with a thickness of 2 pixels, as described in the RedCircle [49]. As for color-based methods [ $*2$ ], we utilize a green color with a transparency level of 0.5 following CPT [61]. Next, we ablate the standard deviation of the Gaussian blur kernel for blur-based prompting [ $*4$ ] (Fig. 5), and a value of 100 achieves the best. More ablation study details on the prompting properties are provided in the Supplementary Materials.

#### 4.4 Referring Expression Comprehension

In this section, we compare our FGVP with previous zero-shot methods in Table 3. For fair comparisons, we also implement FGVP upon the original codebases of each compared method, namely CPT [61] and ReCLIP [50].

We conduct experiments following consistent settings with each compared work. To be specific, with the CPT and our codebase, we focus on individual visual prompting performance without post-processing. We use proposals from UNINEXT and MAttNet to demonstrate the robustness of our enhancements. It’s important to note that different proposal selections solely affect the box candidates, which are equitably shared among all the comparison prompting methods. Next, with the ReClip codebase, ReClip employs cropping and colorful boxes as visual prompts, with default spatially-relations post-processing. To ensure a fair comparison, we first add cropping as an ensemble to all experiments. Next, to facilitate comparison with RedCircle (which inherently uses Score Subtraction as post-processing and primarily ensembles based on three circle prompts), we adopt the same three types of prompt formats but based on semantic masks. Finally, we explore higher performance possibilities. The preprocessing procedure for text inputs, including the prefix and clear-text principle, remains consistent across all codebases. Additionally, we compare zero-shot



Visual Prompt	PACO	RefCOCO	RefCOCO+	RefCOCOg
Crop	16.5	17.7	21.6	34.3
Keypoint	11.9	16.7	18.5	19.7
Circle	17.4	24.9	29.8	32.4
Colorful Mask	15.2	24.1	21.4	18.6
Blur Reverse Mask	<b>18.3</b>	<b>40.8</b>	<b>44.9</b>	<b>49.6</b>

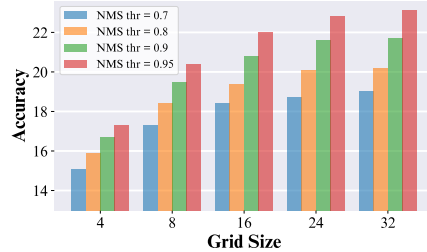


Table 4: Accuracy of the part detection with ViT-L on the validation set of each benchmark. The best result is in **bold**. Figure 6: Ablation study on the NMS threshold and grid size.

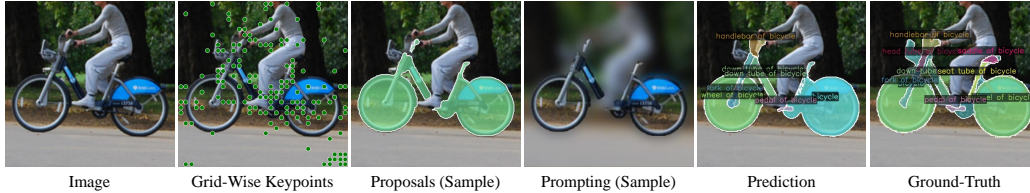


Figure 7: Visualization of the candidate grid-wise keypoints, the proposals, the visual prompting image, and the predicted results in part detection.

referring accuracy under unified CLIP models. Unless otherwise stated, all existing method results are reported according to their original papers.

Table 3 shows that the single fine-grained visual prompt, i.e., Blur Reverse Mask can surpass previous works. With a ViT-L model, our FGVP surpasses RedCircle by an average of 3.4% accuracy in our codebase and 5.5%~8.1% with the CPT [61] codebase. Further, we implement FGVP under the ReCLIP [50] codebase, which investigates the ensemble of multiple models, prompts, and post processing. The results show that the improvement brought by FGVP is orthogonal to the ensemble techniques. Under equal comparisons, our FGVP shows better performance than previous works with a consistent gain of an average of  $\sim 3\%$  and a max of 12.5% in the RefCOCO+ testA set.

#### 4.5 Part Detection

The PACO [44] dataset features annotations for boxes and masks for common objects and their corresponding parts. For the part detection task, models need to locate the part within its object. Different from the referring task, there is no prior information indicating where the parts are. Our proposed pipeline (Fig. 3) is capable of performing zero-shot part detection without box proposals and utilizing only image inputs in these circumstances. Different from the localization keypoints operation employed in RedCircle [40] which only predicts the center location, we instead predict precise semantic masks of the target. Same with the metric in referring expression comprehension, a predicted box is considered correct only when the intersection over union with the ground truth box exceeds 0.5. As shown in Table 4, our proposed method, FGVP, outperforms other coarse prompts for part detection. Notably, we set the grid size to 16 along one side of the image and used an NMS threshold of 0.7 by default. However, better performance can be achieved by including more proposals through the use of a larger grid size and NMS threshold. We conduct an ablation study on them by varying one while fixing the other, as illustrated in Fig. 6. A visualization of the FGVP results is depicted in Fig. 7.

In addition, the referring expression comprehension task can be seen as part detection (each referring instance can be seen as a part of the image) when no prior box proposals are provided. We conducted zero-shot experiments on the validation set of RefCOCO, RefCOCO+, and RefCOCOg datasets, utilizing only images as inputs. As shown in Table 4, the Blur Reverse Mask Prompting without prior box proposals even surpasses certain coarse visual prompting methods with box proposals.

#### 4.6 Limitations

Firstly, FGVP takes longer for inference than other methods because it involves the segmentor to produce semantic masks. To be specific, we compare the inference costs in terms of computation and

Method	SAM scale	Mask-filter	CUDA Memory	Inference Time	IPS	Acc
Crop	–	–	0.91 GB	4.49 min	5.03	45.3
RedCircle [49]	–	–	0.91 GB	4.00 min	5.64	48.9
FGVP (ours)	base	✗	1.32 GB	5.20 min	4.34	51.7
		✓	1.32 GB	27.47 min	0.82	52.1
	large	✗	2.14 GB	6.29 min	3.59	51.0
		✓	2.14 GB	27.49 min	0.82	52.2
	huge	✗	3.42 GB	7.34 min	3.08	51.9
		✓	3.42 GB	28.02 min	0.81	52.8

Table 5: Comparisons of inference cost. **IPS**: Image per GPU second.

speed between our method and others. Further, we conduct an ablation study on the scalability of SAM. Notably, the post-processing technique to filter small disconnected regions and holes in masks can further improve performance at the cost of speed. Disabling the mask-filter post-processing will greatly improve the speed without losing too much performance (Table 5). Experiments are run on RefCOCO with a CLIP pre-trained ViT-L/14@336px on 8× NVIDIA A100. Above all, speeding up the architecture is an important direction for future improvement.

Secondly, the current implementation does not couple the visual prompt with a specifically designed language prompt. Therefore, the image-text alignment comprehension ability of VLM has not been fully explored appropriately. Another consideration is that there are more possible tasks that can adopt the proposed method for zero-shot transfer, such as referring image segmentation. We leave it to our future work.

## 5 Conclusion

In this paper, we focus on the visual prompt, a technique to highlight the target instances in the image content using visible markings such as colorful boxes and circles. The visual prompt is beneficial in invoking potential spatial comprehension within VLMs like CLIP on instance-level tasks. However, existing prompting designs are often too coarse for locating the target instance, leading to unrelated information that may harm performance. Since the topic of visual prompting is rarely explored, we systematically summarize various typical prompting formats and propose Fine-Grained Visual Prompting (FGVP), which utilizes precise semantic masks of target instances derived via Segment Anything (SAM). We discover that the Blur Reverse Mask prompting, which blurs the background, achieves the best performance. Furthermore, we construct two zero-shot classification architectures for regular referring expression comprehension tasks using boxes as prior proposals and for part detection utilizing only input images. We evaluate the effectiveness of FGVP on referring expression comprehension and achieve state-of-the-art (SOTA) performance.

## Acknowledgement

This project is supported by the National Key R&D Program of China (2022ZD0116302), the Fundamental Research Funds for the Central Universities (070-63233084), the Young Scientists Fund of the National Natural Science Foundation of China (Grant No. 62206134), and the Tianjin Key Laboratory of Visual Computing and Intelligent Perception (VCIP). Computation is partially supported by the Supercomputing Center of Nankai University (NKSC). Note that Lingfeng Yang and Jian Yang are with Jiangsu Key Lab of Image and Video Understanding for Social Security, and Key Lab of Intelligent Perception and Systems for High-Dimensional Information of Ministry of Education, Nanjing University of Science and Technology, Nanjing, 210094, P.R. China, while Lingfeng Yang and Xiang Li are with IMPlus@PCALab.

## Broader Impacts

Further research and careful consideration are necessary when utilizing this technology, as the presented proposed method relies on statistics derived from training datasets that may possess biases and could potentially result in negative societal impacts.

## References

- [1] Jean-Baptiste Alayrac, Jeff Donahue, Pauline Luc, Antoine Miech, Iain Barr, Yana Hasson, Karel Lenc, Arthur Mensch, Katherine Millican, Malcolm Reynolds, et al. Flamingo: a visual language model for few-shot learning. *NeurIPS*, 2022.
- [2] Hyojin Bahng, Ali Jahanian, Swami Sankaranarayanan, and Phillip Isola. Exploring visual prompts for adapting large-scale models. *arXiv preprint arXiv:2203.17274*, 2022.
- [3] Hanoona Bangalath, Muhammad Maaz, Muhammad Uzair Khattak, Salman H Khan, and Fahad Shahbaz Khan. Bridging the gap between object and image-level representations for open-vocabulary detection. *NeurIPS*, 2022.
- [4] Amir Bar, Yossi Gandelsman, Trevor Darrell, Amir Globerson, and Alexei Efros. Visual prompting via image inpainting. *NeurIPS*, 2022.
- [5] Omer Bar-Tal, Dolev Ofri-Amar, Rafail Fridman, Yoni Kasten, and Tali Dekel. Text2live: Text-driven layered image and video editing. In *ECCV*, 2022.
- [6] Tim Brooks, Aleksander Holynski, and Alexei A Efros. Instructpix2pix: Learning to follow image editing instructions. *arXiv preprint arXiv:2211.09800*, 2022.
- [7] Tom Brown, Benjamin Mann, Nick Ryder, Melanie Subbiah, Jared D Kaplan, Prafulla Dhariwal, Arvind Neelakantan, Pranav Shyam, Girish Sastry, Amanda Askell, et al. Language models are few-shot learners. *NeurIPS*, 2020.
- [8] Nicolas Carion, Francisco Massa, Gabriel Synnaeve, Nicolas Usunier, Alexander Kirillov, and Sergey Zagoruyko. End-to-end object detection with transformers. In *ECCV*, 2020.
- [9] Xianjie Chen, Roozbeh Mottaghi, Xiaobai Liu, Sanja Fidler, Raquel Urtasun, and Alan Yuille. Detect what you can: Detecting and representing objects using holistic models and body parts. In *CVPR*, 2014.
- [10] Yen-Chun Chen, Linjie Li, Licheng Yu, Ahmed El Kholy, Faisal Ahmed, Zhe Gan, Yu Cheng, and Jingjing Liu. Uniter: Universal image-text representation learning. In *ECCV*, 2020.
- [11] Bowen Cheng, Alex Schwing, and Alexander Kirillov. Per-pixel classification is not all you need for semantic segmentation. *NeurIPS*, 2021.
- [12] Aakanksha Chowdhery, Sharan Narang, Jacob Devlin, Maarten Bosma, Gaurav Mishra, Adam Roberts, Paul Barham, Hyung Won Chung, Charles Sutton, Sebastian Gehrmann, et al. Palm: Scaling language modeling with pathways. *arXiv preprint arXiv:2204.02311*, 2022.
- [13] Jifeng Dai, Kaiming He, and Jian Sun. Instance-aware semantic segmentation via multi-task network cascades. In *CVPR*, 2016.
- [14] Yu Du, Fangyun Wei, Zihe Zhang, Miaojing Shi, Yue Gao, and Guoqi Li. Learning to prompt for open-vocabulary object detection with vision-language model. In *CVPR*, 2022.
- [15] Yuxin Fang, Wen Wang, Binhui Xie, Quan Sun, Ledell Wu, Xinggang Wang, Tiejun Huang, Xinlong Wang, and Yue Cao. Eva: Exploring the limits of masked visual representation learning at scale. *CVPR*, 2023.
- [16] Chengjian Feng, Yujie Zhong, Zequn Jie, Xiangxiang Chu, Haibing Ren, Xiaolin Wei, Weidi Xie, and Lin Ma. Promptdet: Towards open-vocabulary detection using uncurated images. In *ECCV*, 2022.
- [17] Ross Girshick, Jeff Donahue, Trevor Darrell, and Jitendra Malik. Rich feature hierarchies for accurate object detection and semantic segmentation. In *CVPR*, 2014.
- [18] Ke Gong, Xiaodan Liang, Yicheng Li, Yimin Chen, Ming Yang, and Liang Lin. Instance-level human parsing via part grouping network. In *ECCV*, 2018.
- [19] Ke Gong, Xiaodan Liang, Dongyu Zhang, Xiaohui Shen, and Liang Lin. Look into person: Self-supervised structure-sensitive learning and a new benchmark for human parsing. In *CVPR*, 2017.
- [20] Xiuye Gu, Tsung-Yi Lin, Weicheng Kuo, and Yin Cui. Open-vocabulary object detection via vision and language knowledge distillation. *ICLR*, 2022.
- [21] Kaiming He, Georgia Gkioxari, Piotr Dollár, and Ross Girshick. Mask r-cnn. In *ICCV*, 2017.
- [22] Menglin Jia, Luming Tang, Bor-Chun Chen, Claire Cardie, Serge Belongie, Bharath Hariharan, and Ser-Nam Lim. Visual prompt tuning. In *ECCV*, 2022.

- [23] Aishwarya Kamath, Mannat Singh, Yann LeCun, Gabriel Synnaeve, Ishan Misra, and Nicolas Carion. Mdetr-modulated detection for end-to-end multi-modal understanding. In *ICCV*, 2021.
- [24] Wonjae Kim, Bokyoung Son, and Ildoo Kim. Vilt: Vision-and-language transformer without convolution or region supervision. In *ICML*, 2021.
- [25] Alexander Kirillov, Kaiming He, Ross Girshick, Carsten Rother, and Piotr Dollár. Panoptic segmentation. In *CVPR*, 2019.
- [26] Alexander Kirillov, Eric Mintun, Nikhila Ravi, Hanzi Mao, Chloe Rolland, Laura Gustafson, Tete Xiao, Spencer Whitehead, Alexander C Berg, Wan-Yen Lo, et al. Segment anything. *arXiv preprint arXiv:2304.02643*, 2023.
- [27] Harold W Kuhn. The hungarian method for the assignment problem. *Naval research logistics quarterly*, 1955.
- [28] Christoph H Lampert, Hannes Nickisch, and Stefan Harmeling. Learning to detect unseen object classes by between-class attribute transfer. In *CVPR*, 2009.
- [29] Junnan Li, Dongxu Li, Silvio Savarese, and Steven Hoi. Blip-2: Bootstrapping language-image pre-training with frozen image encoders and large language models. *arXiv preprint arXiv:2301.12597*, 2023.
- [30] Junnan Li, Dongxu Li, Caiming Xiong, and Steven Hoi. Blip: Bootstrapping language-image pre-training for unified vision-language understanding and generation. In *ICML*, 2022.
- [31] Junnan Li, Ramprasaath Selvaraju, Akhilesh Gotmare, Shafiq Joty, Caiming Xiong, and Steven Chu Hong Hoi. Align before fuse: Vision and language representation learning with momentum distillation. *NeurIPS*, 2021.
- [32] Liunian Harold Li, Pengchuan Zhang, Haotian Zhang, Jianwei Yang, Chunyuan Li, Yiwu Zhong, Lijuan Wang, Lu Yuan, Lei Zhang, Jenq-Neng Hwang, et al. Grounded language-image pre-training. In *CVPR*, 2022.
- [33] Xiujun Li, Xi Yin, Chunyuan Li, Pengchuan Zhang, Xiaowei Hu, Lei Zhang, Lijuan Wang, Houdong Hu, Li Dong, Furu Wei, et al. Oscar: Object-semantics aligned pre-training for vision-language tasks. In *Computer Vision–ECCV 2020: 16th European Conference, Glasgow, UK, August 23–28, 2020, Proceedings, Part XXX 16*, pages 121–137. Springer, 2020.
- [34] Yanghao Li, Haoqi Fan, Ronghang Hu, Christoph Feichtenhofer, and Kaiming He. Scaling language-image pre-training via masking. *arXiv preprint arXiv:2212.00794*, 2022.
- [35] Feng Liang, Bichen Wu, Xiaoliang Dai, Kunpeng Li, Yanan Zhao, Hang Zhang, Peizhao Zhang, Peter Vajda, and Diana Marculescu. Open-vocabulary semantic segmentation with mask-adapted clip. *arXiv preprint arXiv:2210.04150*, 2022.
- [36] Tsung-Yi Lin, Michael Maire, Serge Belongie, James Hays, Pietro Perona, Deva Ramanan, Piotr Dollár, and C Lawrence Zitnick. Microsoft coco: Common objects in context. In *ECCV*, 2014.
- [37] Shilong Liu, Zhaoyang Zeng, Tianhe Ren, Feng Li, Hao Zhang, Jie Yang, Chunyuan Li, Jianwei Yang, Hang Su, Jun Zhu, et al. Grounding dino: Marrying dino with grounded pre-training for open-set object detection. *arXiv preprint arXiv:2303.05499*, 2023.
- [38] Jonathan Long, Evan Shelhamer, and Trevor Darrell. Fully convolutional networks for semantic segmentation. In *CVPR*, 2015.
- [39] Junhua Mao, Jonathan Huang, Alexander Toshev, Oana Camburu, Alan L Yuille, and Kevin Murphy. Generation and comprehension of unambiguous object descriptions. In *CVPR*, 2016.
- [40] Rafael Müller, Simon Kornblith, and Geoffrey Hinton. When does label smoothing help? *arXiv preprint arXiv:1906.02629*, 2019.
- [41] OpenAI. Gpt-4 technical report. *arXiv preprint arXiv:2303.08774*, 2023.
- [42] Alec Radford, Jong Wook Kim, Chris Hallacy, Aditya Ramesh, Gabriel Goh, Sandhini Agarwal, Girish Sastry, Amanda Askell, Pamela Mishkin, Jack Clark, et al. Learning transferable visual models from natural language supervision. In *ICML*, 2021.
- [43] Colin Raffel, Noam Shazeer, Adam Roberts, Katherine Lee, Sharan Narang, Michael Matena, Yanqi Zhou, Wei Li, and Peter J Liu. Exploring the limits of transfer learning with a unified text-to-text transformer. *The Journal of Machine Learning Research*, 2020.

- [44] Vignesh Ramanathan, Anmol Kalia, Vladan Petrovic, Yi Wen, Baixue Zheng, Baishan Guo, Rui Wang, Aaron Marquez, Rama Kovvuri, Abhishek Kadian, et al. Paco: Parts and attributes of common objects. *arXiv preprint arXiv:2301.01795*, 2023.
- [45] Aditya Ramesh, Prafulla Dhariwal, Alex Nichol, Casey Chu, and Mark Chen. Hierarchical text-conditional image generation with clip latents. *arXiv preprint arXiv:2204.06125*, 2022.
- [46] Aditya Ramesh, Mikhail Pavlov, Gabriel Goh, Scott Gray, Chelsea Voss, Alec Radford, Mark Chen, and Ilya Sutskever. Zero-shot text-to-image generation. In *ICML*, 2021.
- [47] Shaoqing Ren, Kaiming He, Ross Girshick, and Jian Sun. Faster r-cnn: Towards real-time object detection with region proposal networks. In *NeurIPS*, 2015.
- [48] Taylor Shin, Yasaman Razeghi, Robert L Logan IV, Eric Wallace, and Sameer Singh. Autoprompt: Eliciting knowledge from language models with automatically generated prompts. *arXiv preprint arXiv:2010.15980*, 2020.
- [49] Aleksandar Shtedritski, Christian Rupprecht, and Andrea Vedaldi. What does clip know about a red circle? visual prompt engineering for vlms. *arXiv preprint arXiv:2304.06712*, 2023.
- [50] Sanjay Subramanian, Will Merrill, Trevor Darrell, Matt Gardner, Sameer Singh, and Anna Rohrbach. Re-clip: A strong zero-shot baseline for referring expression comprehension. *arXiv preprint arXiv:2204.05991*, 2022.
- [51] Quan Sun, Yuxin Fang, Ledell Wu, Xinlong Wang, and Yue Cao. Eva-clip: Improved training techniques for clip at scale. *arXiv preprint arXiv:2303.15389*, 2023.
- [52] Richard Szeliski. *Computer vision: algorithms and applications*. Springer Nature, 2022.
- [53] Hugo Touvron, Thibaut Lavril, Gautier Izacard, Xavier Martinet, Marie-Anne Lachaux, Timothée Lacroix, Baptiste Rozière, Naman Goyal, Eric Hambro, Faisal Azhar, et al. Llama: Open and efficient foundation language models. *arXiv preprint arXiv:2302.13971*, 2023.
- [54] Catherine Wah, Steve Branson, Peter Welinder, Pietro Perona, and Serge Belongie. The caltech-ucsd birds-200-2011 dataset. *California Institute of Technology*, 2011.
- [55] Xinlong Wang, Tao Kong, Chunhua Shen, Yuning Jiang, and Lei Li. Solo: Segmenting objects by locations. In *ECCV*, 2020.
- [56] Xinlong Wang, Xiaosong Zhang, Yue Cao, Wen Wang, Chunhua Shen, and Tiejun Huang. Seggpt: Segmenting everything in context. *arXiv preprint arXiv:2304.03284*, 2023.
- [57] Ross Wightman. Pytorch image models. <https://github.com/rwightman/pytorch-image-models>, 2019.
- [58] Fangting Xia, Peng Wang, Liang-Chieh Chen, and Alan L Yuille. Zoom better to see clearer: Human and object parsing with hierarchical auto-zoom net. In *ECCV*, 2016.
- [59] Mengde Xu, Zheng Zhang, Fangyun Wei, Yutong Lin, Yue Cao, Han Hu, and Xiang Bai. A simple baseline for open-vocabulary semantic segmentation with pre-trained vision-language model. In *ECCV*, 2022.
- [60] Bin Yan, Yi Jiang, Jiannan Wu, Dong Wang, Ping Luo, Zehuan Yuan, and Huchuan Lu. Universal instance perception as object discovery and retrieval. *arXiv preprint arXiv:2303.06674*, 2023.
- [61] Yuan Yao, Ao Zhang, Zhengyan Zhang, Zhiyuan Liu, Tat-Seng Chua, and Maosong Sun. Cpt: Colorful prompt tuning for pre-trained vision-language models. *arXiv preprint arXiv:2109.11797*, 2021.
- [62] Licheng Yu, Zhe Lin, Xiaohui Shen, Jimei Yang, Xin Lu, Mohit Bansal, and Tamara L Berg. Mattrnet: Modular attention network for referring expression comprehension. In *CVPR*, 2018.
- [63] Licheng Yu, Patrick Poirson, Shan Yang, Alexander C Berg, and Tamara L Berg. Modeling context in referring expressions. In *ECCV*, 2016.
- [64] Yuhang Zang, Wei Li, Kaiyang Zhou, Chen Huang, and Chen Change Loy. Open-vocabulary detr with conditional matching. In *ECCV*, 2022.
- [65] Ning Zhang, Jeff Donahue, Ross Girshick, and Trevor Darrell. Part-based r-cnns for fine-grained category detection. In *ECCV*, 2014.

- [66] Pengchuan Zhang, Xiujun Li, Xiaowei Hu, Jianwei Yang, Lei Zhang, Lijuan Wang, Yejin Choi, and Jianfeng Gao. Vinvl: Revisiting visual representations in vision-language models. In *CVPR*, 2021.
- [67] Hengshuang Zhao, Jianping Shi, Xiaojuan Qi, Xiaogang Wang, and Jiaya Jia. Pyramid scene parsing network. In *CVPR*, 2017.
- [68] Shiyu Zhao, Zhixing Zhang, Samuel Schulter, Long Zhao, BG Vijay Kumar, Anastasis Stathopoulos, Manmohan Chandraker, and Dimitris N Metaxas. Exploiting unlabeled data with vision and language models for object detection. In *ECCV*, 2022.
- [69] Kaiyang Zhou, Jingkang Yang, Chen Change Loy, and Ziwei Liu. Learning to prompt for vision-language models. *IJCV*, 2022.

## Appendix

### A More Ablations on Visual Prompting Properties

In this section, we provide detailed elaborations on the settings of various visual markers.

#### A.1 Thickness and Color for Line-Based Prompting

The research conducted by Shtedritski et al. [49] highlights the strong performance of the visual prompt featuring a red circle in the referring expression comprehension task. To examine the line-based visual prompting settings, we perform independent ablation experiments on line thickness and color using red circle prompting as a representative. Initially, we conduct an ablation study by varying the thickness from 1 to 5 pixels, keeping the color fixed as red. Similarly, regarding the experiment of line color, the options include  $((255, 0, 0), \text{Red})$ ,  $((0, 255, 0), \text{Green})$ ,  $((255, 255, 0), \text{Yellow})$ ,  $((0, 255, 255), \text{Cyan})$ ,  $((0, 0, 255), \text{Blue})$ , and  $((128, 0, 128), \text{Purple})$ . It's worth noting that CPT [61] previously conducted a grid search in the RGB space and determined the best color to be a dark red with RGB values of  $(240, 0, 30)$ , referred to as *CPT-Red* in our experiment. In addition, we maintain a constant thickness of 2 pixels during the color ablation test. Finally, based on the analysis in Fig. A8 and Fig. A9, we observe that a thickness of 2 pixels and a red color achieve the highest overall performance.

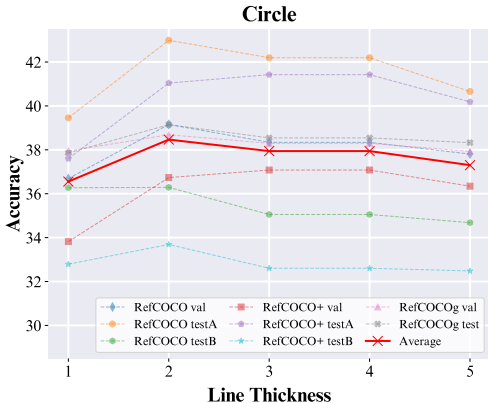


Figure A8: Ablation study on the line thickness.

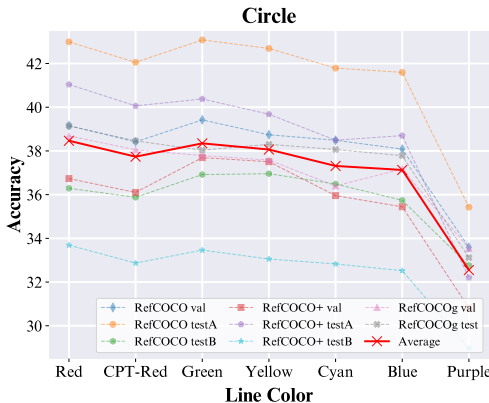


Figure A9: Ablation study on the line color.

#### A.2 Transparency and Color for Color-Based Prompting

For color-based prompting, such as in CPT [61], we consider two hyperparameters of the mask, namely transparency and color. Initially, we set the color to green and vary the transparency from 0.1 to 0.9 with a step of 0.1. Next, with a constant transparency of 0.5, we explore different candidate colors, which are used in the experiments of line-based prompts. Fig. A10 demonstrates that the transparency ranging from 0.3 to 0.5 achieves the best results. Since it effectively highlights the targets without causing excessive interference to the target information. Meanwhile, in Fig. A11, we observe that the impact of color on average accuracy is relatively minor compared to other hyperparameters. Surprisingly, the experiment reveals that the yellow mask achieves the best overall result across 8 benchmarks.

#### A.3 Image Preprocessing

Image preprocessing (Fig. A12) is a crucial but often overlooked aspect in visual prompting techniques used alongside VLMs, such as CLIP [42], for image-text alignment prediction. Typically, CLIP expects input images to be square, whereas most of the natural images in datasets are rectangular. Consequently, these images require preprocessing before being fed into the model. Previous studies [50, 49, 61] have primarily resized rectangular images into squares. However, this approach may result in object stretching and deformation. As a result, it may cause the semantic information

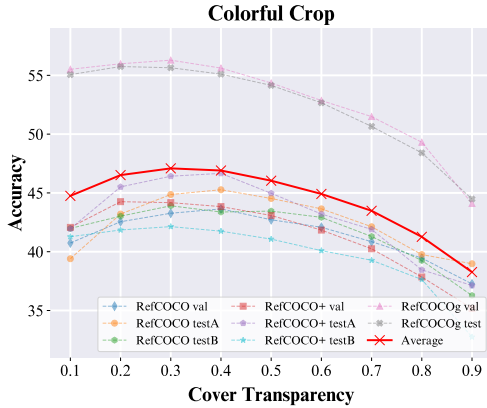


Figure A10: Ablation study on the cover transparency.

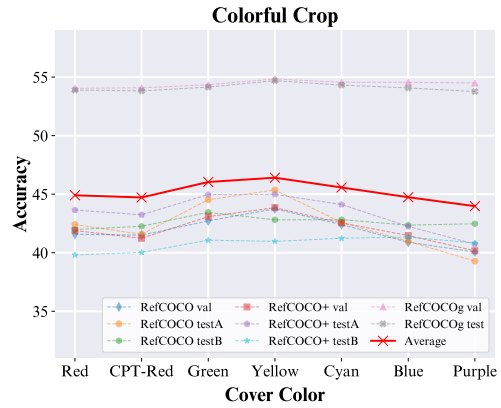


Figure A11: Ablation study on the cover color.

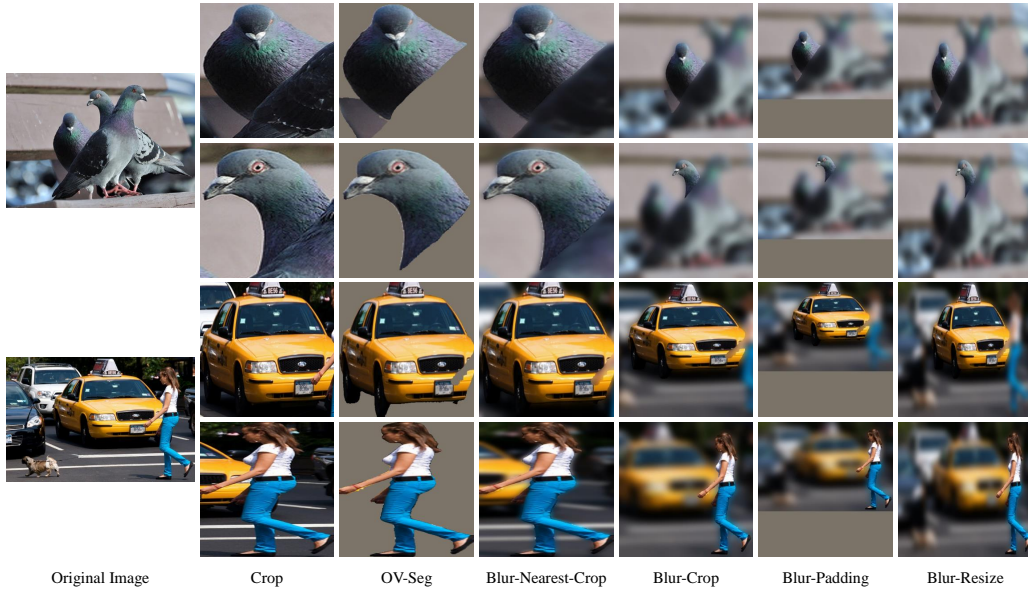


Figure A12: Visualization of different image preprocessing operations aimed at transforming the prompted image into a square format that is compatible with CLIP inputs.

to deviate from its original meaning. Additionally, OV-Seg [35] investigate the open-vocabulary semantic segmentation by first generating cropped instances and subsequently applying grayscale masking to eliminate the background. This work introduces mask engineering, which aims to address the performance bottleneck resulting from masked images featuring a gray background. Then, it finetunes the CLIP to adapt for masked images, so that the accuracy and effectiveness of open-vocabulary semantic segmentation can be improved. However, we have empirically demonstrated that it may be unnecessary to introduce the incompatible background. By applying a single blur operation, we can retain more spatial relevance information. Moreover, since the images are blurred, they

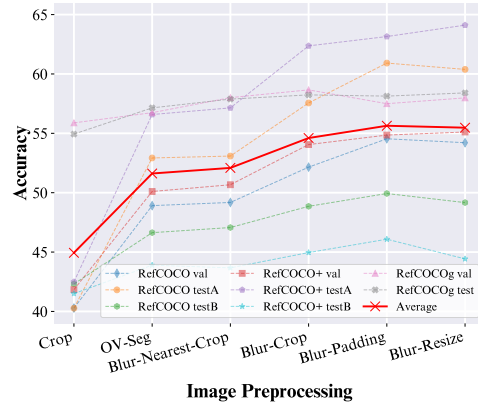


Figure A13: Ablation study on the image preprocessing.



may have a relatively minor impact on the recognition ability of CLIP on the target. Further, some instances may not experience severe deformation compared to previous preprocessing operations, as illustrated by the pedestrian in Fig. A12. Notably, the “Bokeh” paradigm subtly corresponds to the web-scaled data used in CLIP training, where CLIP may possess embedded knowledge for recognizing blurred images. As shown in Fig. A13, blur-based prompting achieves overall better performance compared to crop-based and grayscale-based OV-Seg prompting. It is worth noting that equipping Blur Reverse Mask with further padding or resizing achieves the best performance.

#### A.4 Robustness of Mask Preciseness

Given relatively accurate masks or corresponding circles, we investigate to analyze the impact of different mask preciseness on zero-shot performance. To explore this, we introduce a parameter called the “expand scale”, which allows us to adjust the size of the mask around the target by expanding or shrinking it. When the expand scale is less than 1, it indicates shrinking towards the center. The visualization of this process is depicted in Fig. A14. Regardless of whether the mask is expanded or shrunk, it leads to inaccurate captioning of the target, resulting in a decrease in performance (Fig. A14). This emphasizes the significance of having a precise and detailed mask. To conduct a control experiment, we also applied the same operation to the Blur Reverse Circle. Similarly, the best performance is achieved when the scale is set to 1. An important reason is that a larger range introduces more background noise, while a smaller range leads to a loss of target information, both of which lead to a decrease in performance, as illustrated in Fig. A15.

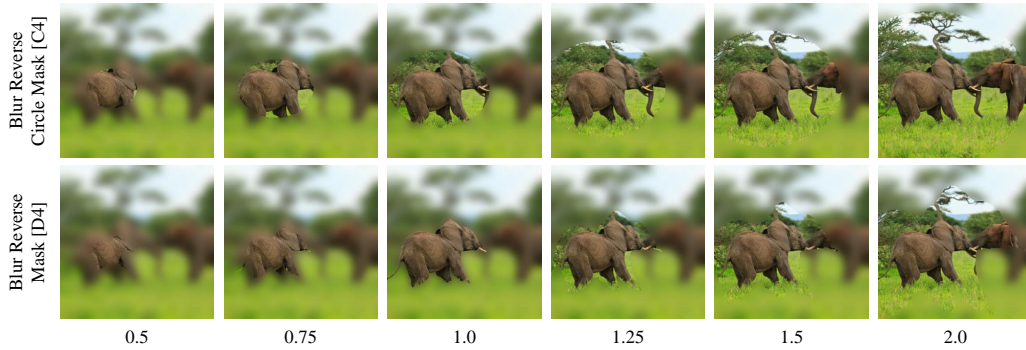


Figure A14: Visualization of blurring images with masks of different preciseness adjusted by an expand scale coefficient, denoted in the bottom. The “1.0” is the expand scale of the baseline for each visual prompting.

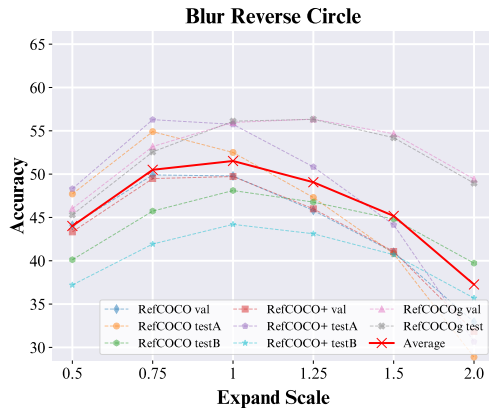


Figure A15: Ablation study on the robustness of the mask preciseness under Blur Reverse Circle.

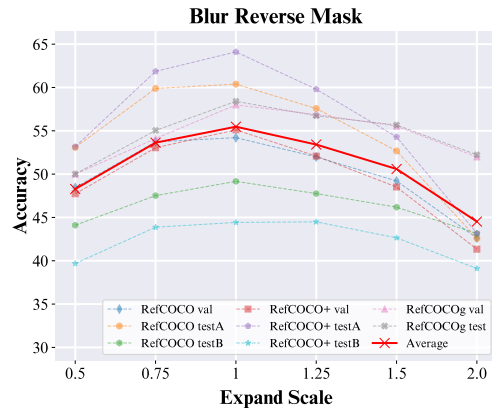


Figure A16: Ablation study on the robustness of the mask preciseness under Blur Reverse Mask.

## B Visual Prompting Expertise

In terms of general object detection tasks, cropping may be preferable since labels are frequently only relevant to the target image. As a result, it is critical to minimize background noise as much as possible. In the case of part detection and referring expression comprehension task, positive prompting or negative prompting with the preservation of more global information is more appropriate. This is because local features, such as a dog’s tail, are difficult to recognize in isolation. Regarding the referring expression comprehension task, it is similar to the caption and may contain information about the target object’s relative relationship with other objects. When it is difficult to identify the target object, information about its relative position can be utilized for zero-shot localization.

## C More Visualizations

In this section, we present the visualizations of the Fine-Grained Visual Prompting (FGVP) results for the referring expression comprehension task, as shown in Fig. A17. The captions are displayed in the lower-left corner of the displayed images. Additionally, image grounding results on the COCO dataset using input images and their possible corresponding labels are shown. (Fig. A18). The results reflect the alignment between instances and labels within the figure. Categories with the same labels are indicated using identical colors, and all candidates are generated from the Segment Anything method [26] under the framework we implemented.

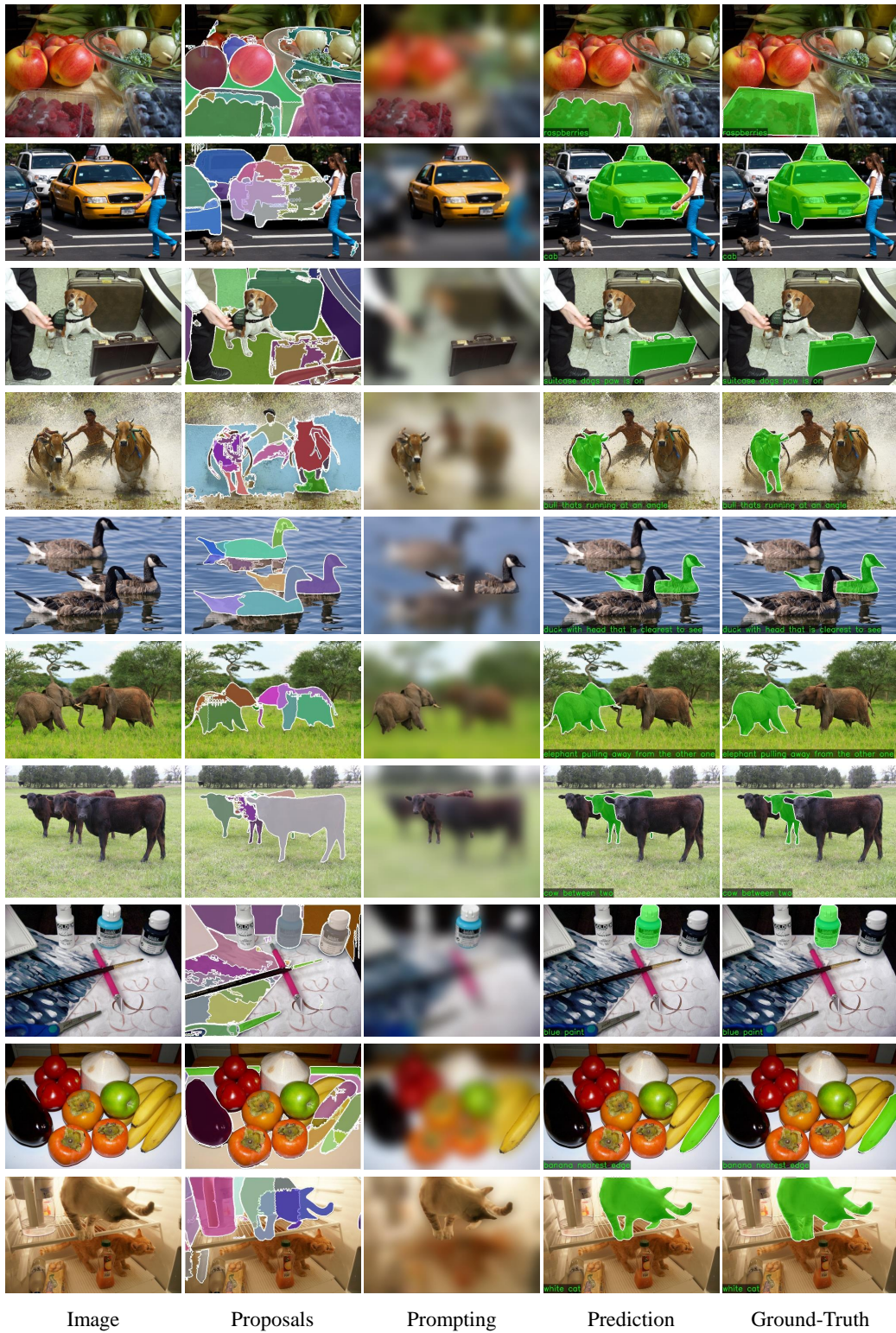
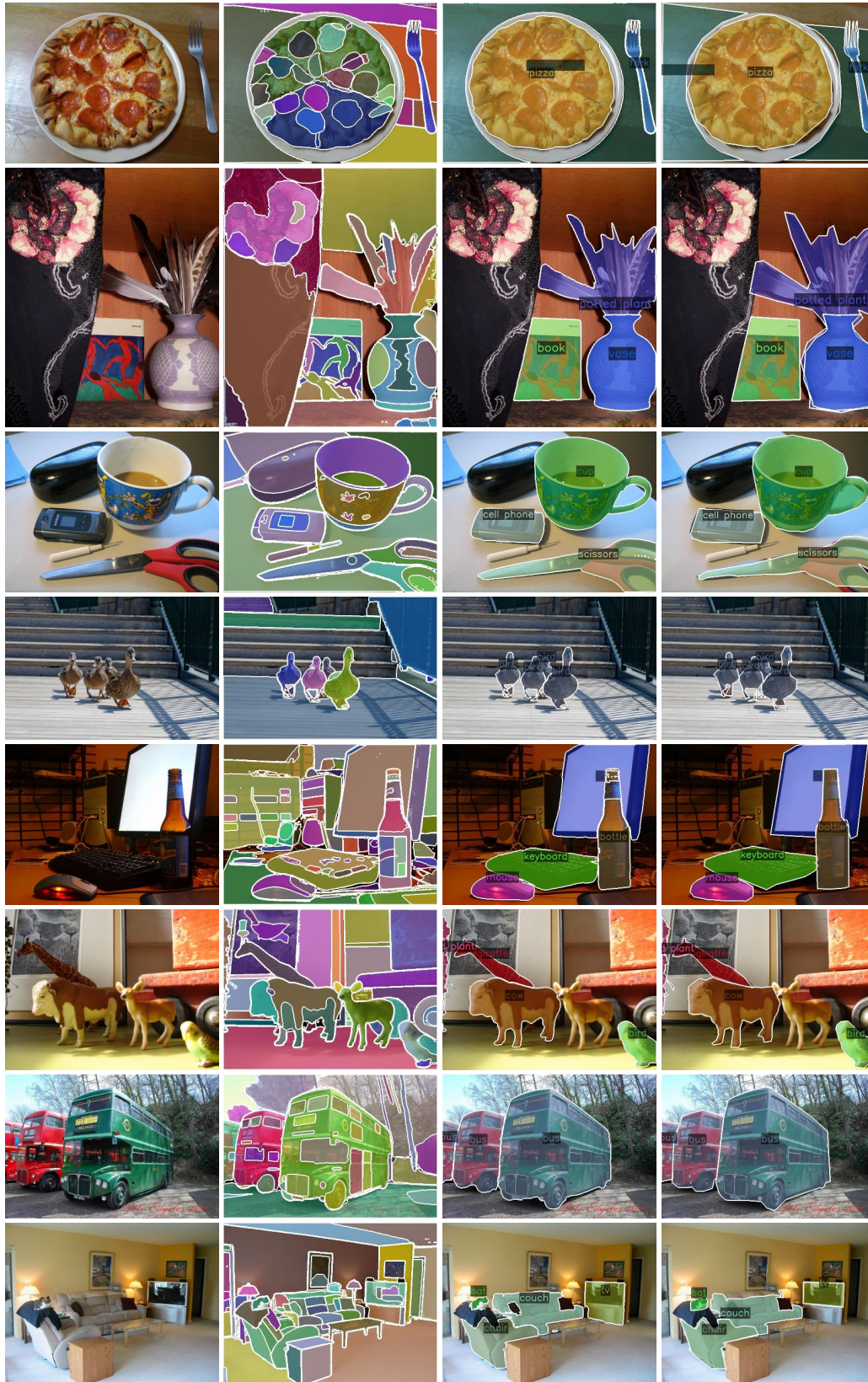


Figure A17: Visualization of FGVP results on the referring expression comprehension task under the RefCOCO, RefCOCO+, and RefCOCOg datasets.



Image

Proposals

Prediction

Ground-Truth

Figure A18: Visualization of FGVP results under the COCO dataset.